Nuclear Engineering and Design 74 (1982) 173–182
North-Holland Publishing Company

THERMO-MECHANICAL CONSTITUTIVE EQUATIONS FOR THE DESCRIPTION OF SHAPE MEMORY EFFECTS IN ALLOYS

A. BERTRAM

2. Institut für Mechanik, Technische Universität Berlin, Berlin (West), Germany

Received 10 January 1983

A class of alloys show 'shape memory effects' which make them applicable for many tasks. For them it is possible to remove imposed deformations nearly entirely by heating. By cooling the material again under constant loads one nearly obtains the old deformations again. It will be shown that this effect as well as others can be described in three dimensions by means of an extended classical theory of plasticity. Two temperature-dependent yield criteria are used which respond under different conditions. For the one-dimensional case the constitutive equations can be simulated by a rheological model. An algorithm makes the material functions applicable for engineering purposes. Numerical results are given for spacial bending of bars.

1. Introduction

Certain metal alloys show thermo-mechanical effects which are in contradiction to what we would customarily expect for metals [1]. A typical and since long wellknown representative of this class is the nickel–titan-alloy 55/45 'Nitinol' (see [2], [3], e.g.). In order to demonstrate such effects, let us, at first, regard the uniaxial tensile test isothermally, at a low temperature (see fig. 1). At the beginning the material behaves like an elastic–plastic one: an elastic leg of the stress–tension curve A is followed by one of plastic yield after reaching a more or less distinct flow limit σ_{F_1}. After complete unloading (C) the plastic deformation ϵ_{pl} remains.

By drawing the specimen again, a small hysteresis in the stress–tension diagram is obtained, which, for most cases, can be neglected for practical reasons, such that

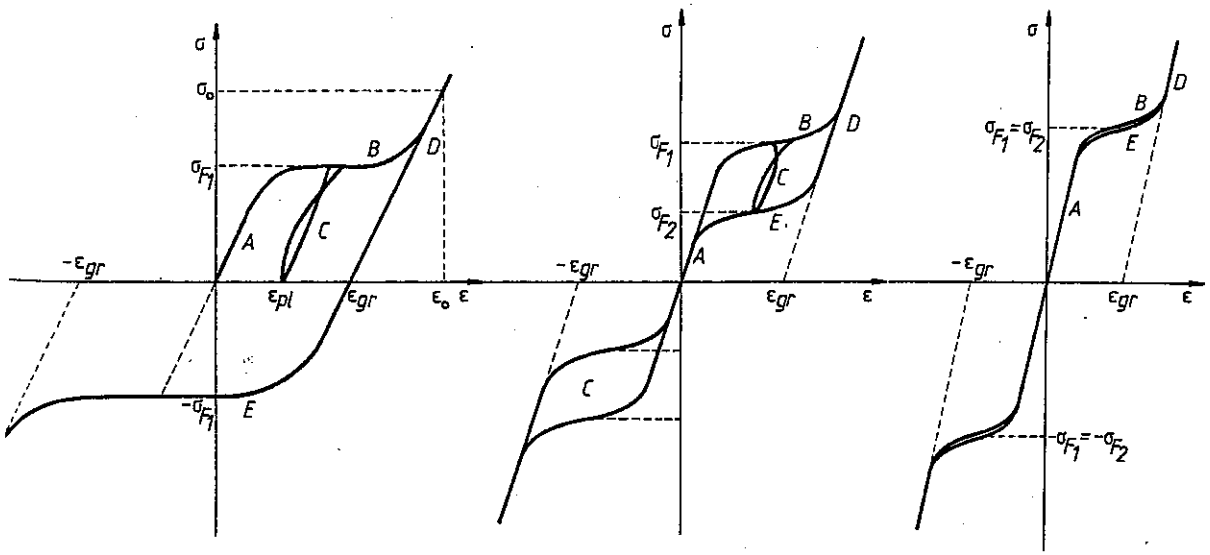

Fig. 1, 2 and 3. Typical stress–strain diagrams for three characteristic temperatures.

0029-5493/82/0000–0000/$02.75

we can assume the existence of an elastic region, as being customary within the classical theory of plasticity. After further deformation the trajectory reaches a second elastic leg D after fulfilling a certain limit condition, indicated by the maximal plastic deformation ϵ_{gr}.

There are still large load increments possible without remarkable additional plastic yield. According to experimental results, the behavior in the presssure test can be assumed as being symmetric to the tensile one in good approximation. If we repeat the tensile test at elevated temperatures, we observe the following effects (see fig. 2):

Effect 1. The elastic stiffness increases with the temperature θ.

Effect 2. The yield limit σ_{F_1} increases with the temperature.

Effect 3. The maximal plastic deformation ϵ_{gr} varies according to temperature changes. In most cases it decreases under heating.

Effect 4. The yield limit in the pressure part (denoted by $-\sigma_{F_2}$) increases, vanishes, and can be elevated far into the positive quadrant. As a limit it can coincide with the other yield limit σ_{F_1}, and we formaly obtain a (non-linear) elastic behavior in the entire (isothermal) test domain (fig. 3).

Effect 4 causes, as shown in fig. 2, a division into two distinct elastic regions, connected by the elastic path A. According to the tensile–compression symmetry, we have to take into account two temperature dependent flow limits $\sigma_{F_1}(\theta)$ and $\sigma_{F_2}(\theta)$. The so-called *shape memory effect* can be performed by the following procedure: At first, we let the specimen undergo a large deformation $\epsilon_0 = \epsilon_{gr} + \epsilon_{el}$ caused by the stress $\sigma_0 > \sigma_{F_1}$ in part D of fig. 1. If we now keep the stress σ_0 constant and raise the temperature, we observe at a certain temperature θ_1 that the deformation vanishes up to a small rest (fig. 4). By cooling the specimen again, nearly the same form and size will occur at another characteristic temperature θ_2 being lower than θ_1. This shape memory effect can be performed arbitrarily often, a property which makes the material applicable for many technical tasks. We are not dealing with models on the microscale, as done by Müller [4], but instead, our aim is to describe and calculate all these effects by constitutive equations in three dimensions in a manner appropriate for engineering purposes. Therefore, we tried to obtain the most simple theory, valid to describe the above effects in order to reduce the calculational effort. For this reason we restrict our considerations to small deformations, and we will always linearize the functions whenever this is possible.

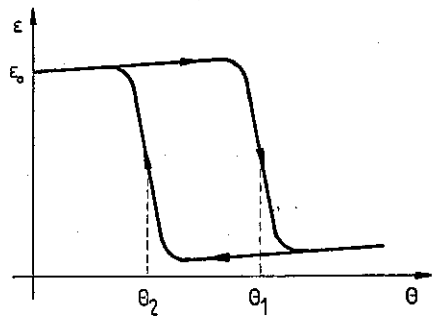

Fig. 4. Strain–temperature diagram under constant loads.

The main problem was the deficiency of (three-dimensional) experimental results. This is the reason why we have to extrapolate rigorously in the most simple way outside the investigated domain. As, in particular, there are very few thermodynamical results, we could not develop a complete set of thermodynamical constitutive relations. The temperature will only be a parameter in our equations.

2. Notations

In general, we use a symbolic tensor-notation for the physical quantities. If a component representation is added, this is done with reference to a cartesian vector base. We denote θ as the temperature, ρ as the density, $\boldsymbol{E}$ as the (linear) Green deformation tensor, $\boldsymbol{D} := \dot{\boldsymbol{E}}$ as the strain rate tensor, and $\boldsymbol{T}$ as the stress tensor. ϵ and σ are the strain and stress, respectively, of the one-dimensional theory. The composition of two tensors $\boldsymbol{A}$ and $\boldsymbol{B}$ is denoted by $\boldsymbol{A} \cdot \boldsymbol{B}$ (or $a_{ij}b_{jk}$). The scalar product is defined as the being trace $\boldsymbol{A} \cdot \cdot \boldsymbol{B} := \mathrm{tr}(\boldsymbol{A} \cdot \boldsymbol{B})$ (or $a_{ij}b_{ji}$). Let $\boldsymbol{A}$ be a symmetric tensor unequal to the zero tensor, we call

$$\|\boldsymbol{A}\| := \sqrt{\mathrm{tr}(\boldsymbol{A} \cdot \boldsymbol{A})}$$

its norm and $\vec{\boldsymbol{A}} := \boldsymbol{A}/\|\boldsymbol{A}\|$ its direction.
Every tensor $\boldsymbol{A}$ can be decomposed uniquely as

$$\boldsymbol{A} = \boldsymbol{A}' + \tfrac{1}{3}\mathrm{tr}(\boldsymbol{A})\mathbf{1}$$

into its (traceless) deviatoric part $\boldsymbol{A}'$ and a real multiple of the identity tensor $\mathbf{1}$. The identity tensor of degree four is $\boldsymbol{I}$, the dyadic product of two tensors $\boldsymbol{A}$ and $\boldsymbol{B}$ is $\boldsymbol{A} \otimes \boldsymbol{B}$.

3. Constitutive equations

At first, we assume that the initial state is undistorted and stress free ('virginal'). We choose the deformation process $E(t)$ with its right-hand time derivative $D(t)$ and the temperature process $\theta(t)$ with its derivative $\dot{\theta}(t)$ as being the independent variables. We decompose the strain rates

$$D = D_{el} + D_{pl}, \tag{1}$$

such that these parts can be (locally) integrated up to the elastic deformations

$$E_{el} = \int_0^t D_{el}(\tau)\mathrm{d}\tau \tag{2}$$

and the plastic deformations

$$E_{pl} = \int_0^t D_{pl}(\tau)\mathrm{d}\tau. \tag{3}$$

By means of the elastic deformation we can determine the actual stress-tensor $T(t)$. This is done by means of a differentiable *stress function*

$$T = F(E_{el}, \theta) \tag{4}$$

such that the stiffness tensor $\partial F/\partial E_{el}$ is everywhere positive definite. The customary interpretation for the plastic deformations E_{pl}, as being those that remain after isothermal unloading, can be given only for low temperatures. The initial values for both of the deformation parts are zero according to the above assumption.

As long as the deformations E(t) are small enough and the state of the material is in the elastic part A (figs. 1, 2, 3), we have

$$D_{pl} = 0 \Leftrightarrow D = D_{el}. \tag{5}$$

This is no longer valid after reaching the elastic limit, modeled by a *yield criterion* in form of a real valued and partwise differentiable function

$$f_1(T, \theta) \tag{6}$$

of stress and temperature. Its kernel is assumed to form a hyperplane in the stress space. Its values shall be negative in the (elastic) interior, vanish at the yield limit, and become positive for larger stress intensities. Those are admissible for this class of materials within part D.

If the yield limit

$$f_1(T, \theta) = 0 \tag{7}$$

is reached, the material will yield under further deformation increments. The direction of yielding shall be determined by a flow rule, whereas the magnitude $\|D_{pl}\|$ of the plastic flow can be calculated by the consistency equation in connection with the stress function (4), as will be shown in section 4.

As an example we impose a normality rule

$$\vec{D}_{pl} = \overrightarrow{\partial f_1(T, \theta)/\partial T} \tag{8}$$

or

$$D_{pl} = \lambda \partial f_1(T, \theta)/\partial T, \quad \lambda \in \mathbb{R}. \tag{9}$$

The further behavior will depend on whether or not strain hardening will occur. We will suggest different types of hardening in section 7. In most cases it is reasonable to neglect hardening effects. If we unload the material, indicated by

$$\dot{f}_1(T(t), \theta(t)) < 0, \tag{10}$$

we will again be in the elastic region C and the plastic deformation will remain constant.

On the other hand, if we remain on the yield surface, the material will be like an elastic–plastic one until the exterior elastic part D (figs. 1, 2, 3) is reached. This is the case if a temperature dependent *plastic limit deformation* ϵ_{gr} is reached. Therefore, we assume a continuous function

$$g(E_{pl}, \theta) = 0 \tag{11}$$

as a limit criterion, such that the material behavior will again be described solely by the stress function (4) if eq. (11) is fufilled, and D_{pl} is zero.

In contrast to traditional theories of plasticity, for memory alloys there exists another yield limit

$$f_2(T, \theta) = 0, \tag{12}$$

again differentiable in parts, whose interior is indicated by negative values for low temperature and by positive ones for high temperatures, such that in the elastic region C (figs. 1, 2)

$$f_{1,2}(T, \theta) < 0 \tag{13}$$

is always valid. The second yield limit is assumed to be in the interior of the first. It shall respond only if the following *response criterion* is fulfilled:

$$E_{pl} \cdot \cdot D_{pl} < 0. \tag{14}$$

This is due to the fact that the plastic yield at the second yield limit generally reduces the plastic deformation. That is why we call this flow *plastic reductional yielding.*

We again need a flow rule for the second limit

yielding, e.g., the normality rule

$$\boldsymbol{D}_{\mathrm{pl}}=\frac{\lambda\partial f_2(T,\theta)}{\partial \boldsymbol{T}},\quad \lambda\in\mathbb{R}. \tag{15}$$

This yielding reduces the plastic deformations and can be sustained until these are completely eliminated. In analogy to eq. (11), we obtain the final condition

$$\boldsymbol{E}_{\mathrm{pl}}=\boldsymbol{0}. \tag{16}$$

In this state the response criterion is automatically contradicted and the material again enters the elastic leg A (figs. 1, 2, 3).

4. Consistency condition and plastic reductional yielding

Necessary conditions for the response of the yield criteria are—besides the response criterion—the validity of the elastic limit condition

$$f_i(T,\theta)=0, \tag{17}$$

as well as its overstepping, if the deformation increment were a pure elastic one:

$$\boldsymbol{D}\equiv\boldsymbol{D}_{\mathrm{el}}. \tag{18}$$

This leads to the *loading condition*

$$\begin{aligned}\dot f_i|_{\boldsymbol{D}_{\mathrm{el}}=\boldsymbol{D}}&=\frac{\partial f_i}{\partial \boldsymbol{T}}\cdot\cdot\,\dot{\boldsymbol{T}}\Big|_{\boldsymbol{D}_{\mathrm{el}}=\boldsymbol{D}}+\frac{\partial f_i}{\partial\theta}\dot\theta\\&=\frac{\partial f_i}{\partial \boldsymbol{T}}\cdot\cdot\left(\frac{\partial \boldsymbol{F}}{\partial \boldsymbol{E}_{\mathrm{el}}}\cdot\cdot\,\boldsymbol{D}_{\mathrm{el}}+\frac{\partial \boldsymbol{F}}{\partial\theta}\dot\theta\right)\Big|_{\boldsymbol{D}_{\mathrm{el}}=\boldsymbol{D}}\\&\quad+\frac{\partial f_i}{\partial\theta}\dot\theta>0.\end{aligned} \tag{19}$$

If both conditions (17) and (19) are fulfilled, plastic yield can occur, and the stresses remain at the flow limit. This is assured by the *consistency condition*

$$\begin{aligned}\dot f_i=0&=\frac{\partial f_i}{\partial \boldsymbol{T}}\cdot\cdot\,\dot{\boldsymbol{T}}+\frac{\partial f_i}{\partial\theta}\dot\theta\\&=\frac{\partial f_i}{\partial \boldsymbol{T}}\cdot\cdot\frac{\partial \boldsymbol{F}}{\partial \boldsymbol{E}_{\mathrm{el}}}\cdot\cdot\,\boldsymbol{D}_{\mathrm{el}}+\frac{\partial f_i}{\partial \boldsymbol{T}}\cdot\cdot\frac{\partial \boldsymbol{F}}{\partial\theta}\dot\theta\\&\quad+\frac{\partial f_i}{\partial\theta}\dot\theta,\end{aligned} \tag{20}$$

which, in connection with eqs. (1) and (9) or eq. (15), emerges to

$$0=\frac{\partial f_i}{\partial \boldsymbol{T}}\cdot\cdot\frac{\partial \boldsymbol{F}}{\partial \boldsymbol{E}_{\mathrm{el}}}\cdot\cdot\left(\boldsymbol{D}-\lambda\frac{\partial f_i}{\partial \boldsymbol{T}}\right)+\left(\frac{\partial f_i}{\partial \boldsymbol{T}}\cdot\cdot\frac{\partial \boldsymbol{F}}{\partial\theta}+\frac{\partial f_i}{\partial\theta}\right)\dot\theta. \tag{21}$$

By assumption, $\partial \boldsymbol{F}/\partial \boldsymbol{E}_{\mathrm{el}}$ is positive definite, and thus the term

$$\frac{\partial f_i}{\partial \boldsymbol{T}}\cdot\cdot\frac{\partial \boldsymbol{F}}{\partial \boldsymbol{E}_{\mathrm{el}}}\cdot\cdot\frac{\partial f_i}{\partial \boldsymbol{T}} \tag{22}$$

is positive, and we can calculate λ explicitly by the equation

$$\lambda=\frac{\dfrac{\partial f_i}{\partial \boldsymbol{T}}\cdot\cdot\dfrac{\partial \boldsymbol{F}}{\partial \boldsymbol{E}_{\mathrm{el}}}\cdot\cdot\,\boldsymbol{D}+\left(\dfrac{\partial f_i}{\partial \boldsymbol{T}}\cdot\cdot\dfrac{\partial \boldsymbol{F}}{\partial\theta}+\dfrac{\partial f_i}{\partial\theta}\right)\dot\theta}{\dfrac{\partial f_i}{\partial \boldsymbol{T}}\cdot\cdot\dfrac{\partial \boldsymbol{F}}{\partial \boldsymbol{E}_{\mathrm{el}}}\cdot\cdot\dfrac{\partial f_i}{\partial \boldsymbol{T}}}. \tag{23}$$

In connection with the loading condition (19), λ is generally positive, if the deformation and/ or the temperature varies. For $i=2$ this leads, in connection with the response criterion, to

$$0>\boldsymbol{E}_{\mathrm{pl}}\cdot\cdot\,\boldsymbol{D}_{\mathrm{pl}}=\boldsymbol{E}_{\mathrm{pl}}\cdot\cdot\,\lambda\partial f_2/\partial T, \tag{24}$$

i.e. the response criterion is equivalent to the condition

$$\boldsymbol{E}_{\mathrm{pl}}\cdot\cdot\frac{\partial f_2}{\partial \boldsymbol{T}}<0, \tag{25}$$

which can be proved more easily in practical calculations.

The role of the response criterion becomes more evident in the one-dimensional case if we plot σ over ϵ_{pl} instead of ϵ, as done in figs. 5 and 6 for two characteristics temperatures. The one-dimensional version of the response criterion

$$\epsilon_{\mathrm{pl}}\frac{\partial f_2}{\partial\sigma}<0 \tag{26}$$

assures, that the yield can occur at 1, 2, 5, and 6, but not at 3, 4, 7, 8. For f_1 we do not need such a condition, as we postulated that the second limit $f_2=0$ lies in the interior of the first. Therefore, 9 and 10 cannot be reached, as the second limit previously prevents an increase of the stress intensities at 1, 2, 5, or 6.

5. Suggestions for the constitutive functions

The following material functions constitute the materials under consideration and these have to be made more concrete:

(1) the stress function (4),

(2) the two yield limits (6) and (12),

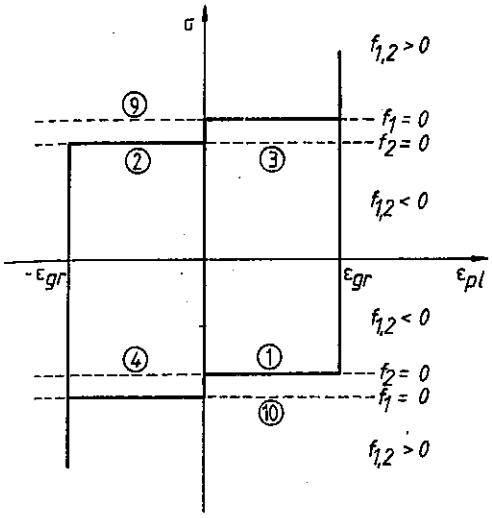

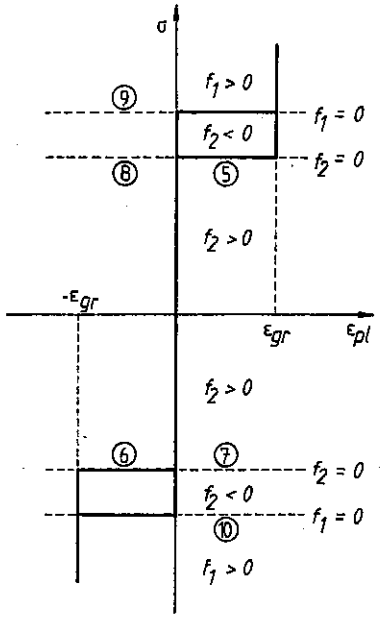

Fig. 5 and 6. The sign of the yield functions in a simple stress–plastic strain dependence. Left: low temperature. Right: high temperature.

(3) the plastic limit criterion (11).

With the remarks from section 1 in mind we will suggest the most simple forms for them:

5.1. We use the linear isotropic Hookean law

$$T = 2G\left[E_{el} + \frac{\nu}{1-2\nu}\operatorname{tr}(E_{el})\mathbf{1} - \frac{1+\nu}{1-2\nu}\alpha\theta\mathbf{1}\right] \tag{27}$$

(G = shear modulus, α = coefficient of thermal expansion, ν = Poissons ratio). This yields

$$\partial F/\partial E_{el} = 2G\left[I + \frac{\nu}{1-2\nu}\mathbf{1}\otimes\mathbf{1}\right], \tag{28}$$

$$\partial F/\partial\theta = -2G\frac{1+\nu}{1-2\nu}\alpha\mathbf{1}. \tag{29}$$

5.2. We suggest for the first flow limit

$$f_1(T,\theta) = \sigma_v(T) - \sigma_{F_1}(\theta), \tag{30}$$

i.e., the difference between a stress intensity σ_v and a temperature-dependent flow stress σ_{F_1}.

As long as there are no contradictive experimental results we choose for σ_v according to Huber and v. Mises

$$\sigma_v = \sqrt{\tfrac{3}{2}}\,\|T'\|. \tag{31}$$

σ_{F_1} is the simplest case a linear function of the temperature

$$\sigma_{F_1}(\theta) = \gamma_1\theta + \delta_1, \quad \gamma_1, \delta_1 > 0, \tag{32}$$

The second yield criterion is chosen to be

$$f_2(T,\theta) = -\operatorname{sgn}\left[\sigma_{F_2}(\theta)\right]\left[|\sigma_v(T)| - |\sigma_{F_2}(\theta)|\right], \tag{33}$$

wherein

$$\sigma_v(T) = \sqrt{\frac{3}{2}}\,\|T'\| \tag{34}$$

is, and $\sigma_{F_2}(\theta)$ increases with the temperature and σ_{F_2} is negative for low temperatures and positive for high ones.

In general

$$\sigma_{F_2} \le \sigma_{F_1}, \tag{35}$$

must be valid. As a simple example we take

$$\sigma_{F_2}(\theta) = \gamma_2\theta - \delta_2 \quad \text{with } \gamma_2, \delta_2 > 0. \tag{36}$$

The reader shall not be worried by the fact that f_2 is not differentiable at $\sigma_{F_2} = 0$, as the derivation exists everywhere else and we could take the upper limit at this point. We obtain the following relations:

$$\frac{\partial f_1}{\partial T} = \sqrt{\frac{3}{2}}\,\frac{T'}{\|T'\|};$$

$$\frac{\partial f_1}{\partial \theta} = -\gamma_1;$$

$$\frac{\partial f_2}{\partial T} = -\operatorname{sgn}\left[\sigma_{F_2}(\theta)\right]\sqrt{\frac{3}{2}}\,\frac{T'}{\|T'\|};$$

$$\frac{\partial f_2}{\partial \theta} = +\gamma_2. \tag{37}$$

5.3. We suggest for g

$$g(E_{pl}, \theta) = \sqrt{\tfrac{2}{3}}\,\|E_{pl}\| - \epsilon_{gr}(\theta) \tag{38}$$

with

$$\epsilon_{gr}(\theta) = \gamma_3\theta + \delta_3, \tag{39}$$

such that the norm of the plastic deformation is restricted in a temperature dependent way.

By the above function we constitute an isotropic (in the sense of [6]) and rate-independent material (in the sense of [5]).

6. The shape memory effect

In order to show that our material model can perform the shape memory effect, we consider a material element without strain hardening and thermal expansion ($\alpha = 0$) and assume, for simplicity, that ϵ_{gr} does not depend on the temperature. We impose a large deformation ϵ_0 at a low temperature for the one dimensional case see fig. 7—such that ϵ_{gr} and the exterior elastic branch has already been reached. Then we hold the reached stress σ_0 constant for the rest of the test. If we heat the element up, both elastic limits increase. If the first limit reaches σ_0, no yield will occur, as $g = 0$. But if the second limit has reached σ_0, the response criterion (25) is fulfilled, and, according to eq. (19) and $\dot{\theta} \neq 0$, the plastic reductional yielding will occur (see fig. 8), in our case discontinuous as a deformation jump to $\epsilon_{pl} = 0$. By further heating the state remains at $\epsilon_{pl} = 0$. If we cool the specimen afterwards it will pass the second elastic limit unaffected, as the response criterion is not fulfilled if $\epsilon_{pl} = 0$. However, if the first elastic limit is at σ_0, ϵ_{pl} jumps back from zero to ϵ_{gr} and remains there. If we plot the total strain ϵ over the temperature θ we obtain fig. 9.

Notice that the strain can be discontinuous in force/temperature controlled tests, whereas the stress is always continuous in strain/temperature controlled tests. We are familiar to this fact from traditional plasticity. Of course, the two deformation discontinuities in fig. 9 can be avoided if we assume strain hardening. In fig. 10 we plotted the diagram for a linear, and in fig. 11 for a non-linear hardening law. If, moreover, we assume an appropriate temperature dependence of ϵ_{gr} and/or a thermal expansion ($\alpha > 0$) we can describe the behavior of fig. 4.

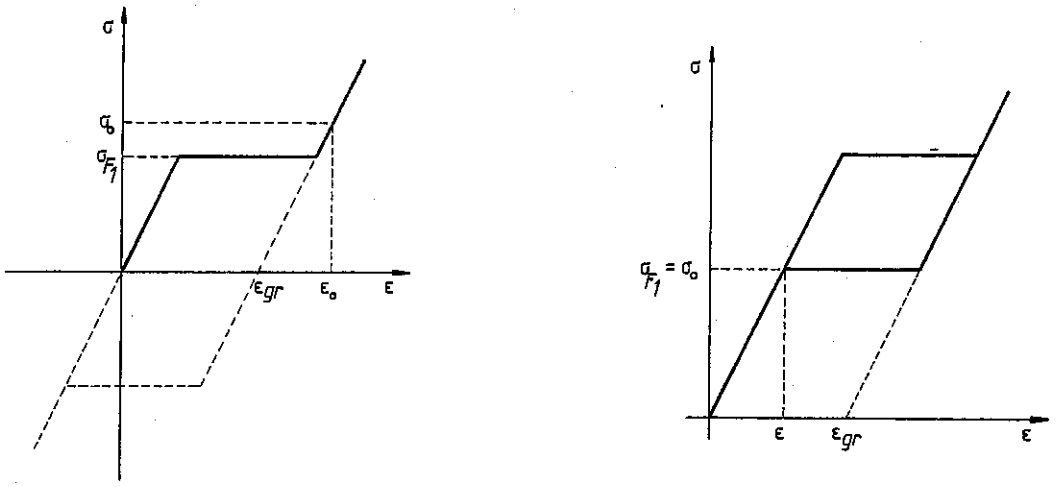

Fig. 7 and 8. The shape memory effect. The stress-strain diagram at a low (left) and at an elevated temperature (right).

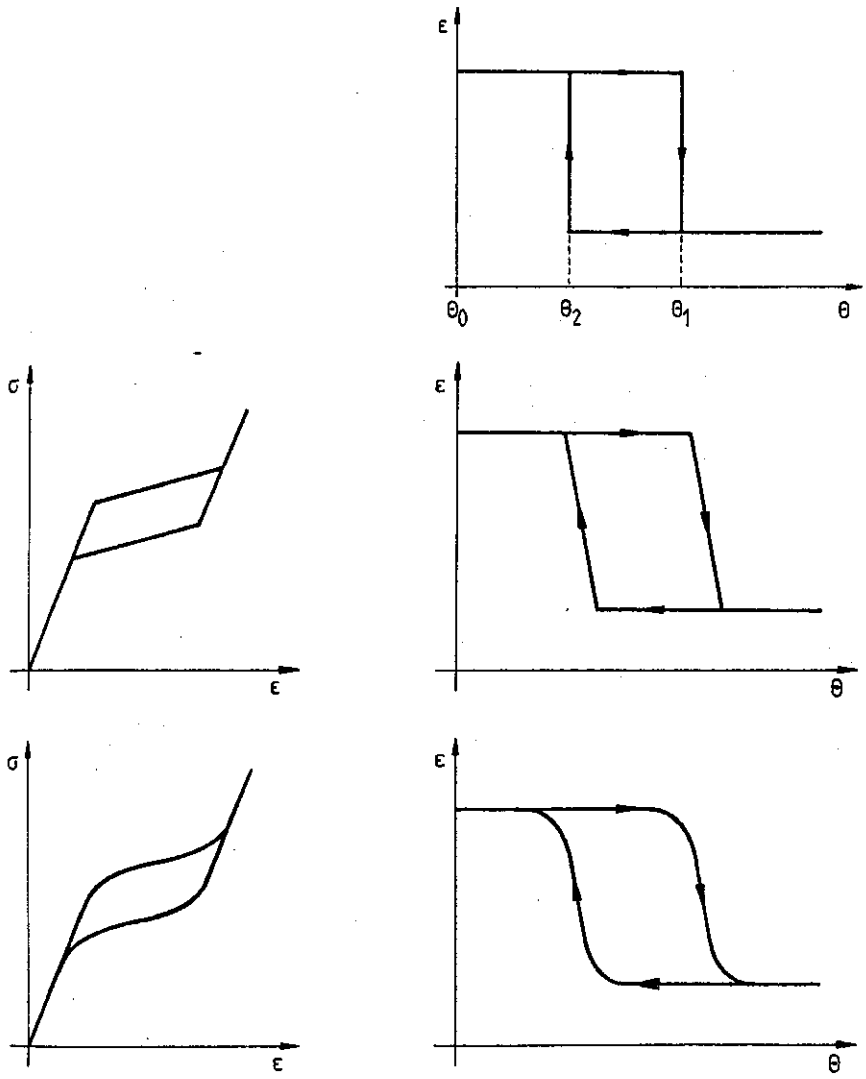

Fig. 9–11. The shape memory effect for different types of strain hardening. Fig. 9 (top): no hardening. Fig. 10 (middle): linear hardening. Fig. 11 (bottom): non-linear hardening.

7. Strain-hardening models

Usually the experimental plots in the region B (figs. 1, 2, 3) show many peaks and unregularities, so that we have to smooth them rigorously for calculational purposes. Although the non-hardening theory as described above has emerged as being practical and satisfactory in most cases, it is possible to add hardening mechanisms. The following concepts are available.

7.1. Kinematic hardening

It is described by a function that maps every plastic deformation process into a symmetric tensor V in a rate-independent way, such that the elastic limits are

$$f_i(T - V, \theta) = 0. \tag{40}$$

In the Huber-v. Mises-version V is deviatoric, and the

stress intensity is given by

$$\sigma_v = \sqrt{\tfrac{3}{2}}\,\|T' - V\|. \tag{41}$$

V can, e.g., depend on the plastic deformation $\|E_{pl}\|$ or on the dissipative work

$$w_{pl} = \int_0^t T \cdot \cdot D_{pl}\,d\tau. \tag{42}$$

7.2. Isotropic hardening

The elastic limits depend, apart from the temperature, on a scalar hardening-parameter Δ, which is a rate-independent function of $\|E_{pl}\|$ or w_{pl}, e.g. We set

$$\sigma_{F_i}(\theta, \Delta). \tag{43}$$

7.3. Combined hardening

It can be useful to use both concepts simultaneously. However, for this generalization we have to pay a remarkable extend of the calculational effort.

8. A rheological model

As the material was entirely idealised by elastic and plastic parts, we can model it by elastic springs (Hookean elements) and dry friction elements (de St.-Venant elements), as done in fig. 12. The two de St.-Venant elements at the ends of the model have the same temperature dependent friction coefficients $\mu(\theta)$, i.e., they are in equilibrium for forces less than μ, and they can move on a length of ϵ_{gr} between two limit stops if the force equals μ. They represent the plastic strain ϵ_{pl}, in a way, that one of the elements is generally at a limit stop. The spring in the middle with a temperature dependent stiffness $C(\theta)$ is activated on the central and exterior elastic legs of figs. 1 and 2. The other two symmetrically located springs are weak and prestrained, one under pressure and the other under tension. Their stiffnesses are temperature dependent too. If their forces are assumed to be independent of their length differences, we have no strain hardening.

We evaluate for the first elastic limit

$$\sigma_{F_1} = K(\theta) + \mu(\theta) \tag{44}$$

and for the second

$$\sigma_{F_2} = K(\theta) - \mu(\theta)$$

(see fig. 13). K and μ increase and decrease, respectively, with the temperature. The two temperature extremes are:

$$\begin{aligned} &(1)\ \text{very low temperature: } K = 0 \Rightarrow \sigma_{F_1} = -\sigma_{F_2}, \\ &(2)\ \text{very high temperature: } \mu = 0 \Rightarrow \sigma_{F_1} = \sigma_{F_2}. \end{aligned} \tag{45}$$

In the absence of strain hardening, energy is stored in the central spring with the amount of $\frac{1}{2}C\epsilon_{el}^2$ and in one of the prestrained springs with $K\epsilon_{pl}$, whereas the dissipation occurs in one of the de St.-Venant elements.

9. An algorithm

Let $E(t)$ and $\theta(t)$ be piecewise continuously differentiable deformation and temperature processes, respectively. Then we can calculate the responding stress process, if all constitutive functions are identified. For this calculation we can apply the given algorithm, which turns out to work with rather small numerical effort. In it the time t advances, until the response to one request changes.

A discretization in time and an incremental procedure seem to be appropriate. We use quotients of differences instead of differential quotients and work out the integrations as pure sums. This algorithm was applied for the numerical results in the next section.

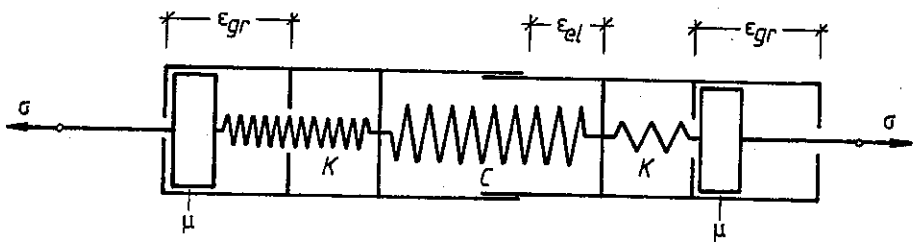

Fig. 12. Rheological model.

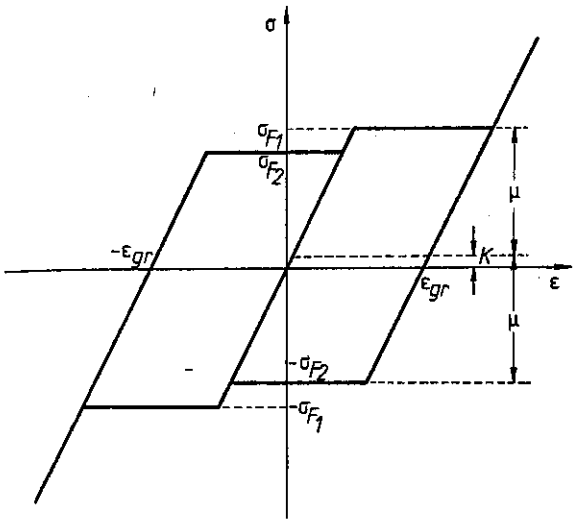

Fig. 13. Characteristic values in the stress–strain diagram.

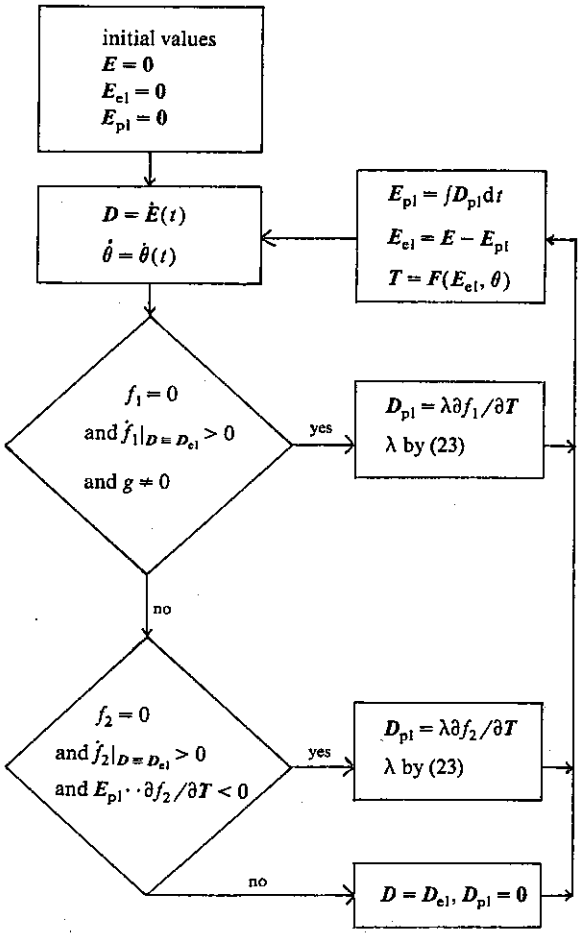

10. Applications

By means of these constitutive equations, we simulated three dimensional tests on the computer, as well as one dimensional applications, especially, the spacial bending of bars. Fig. 13 shows the one dimensional form of the stress tension behavior, by which we implemented a finite element program and calculated the bending moments isothermally in dependence of the curvature for three characteristic temperatures, as

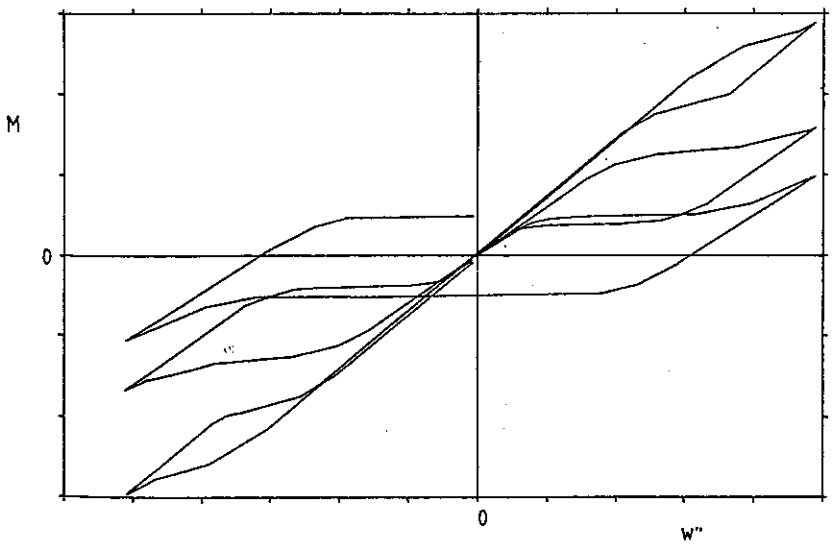

Fig. 14. Bending of a bar at three temperatures.

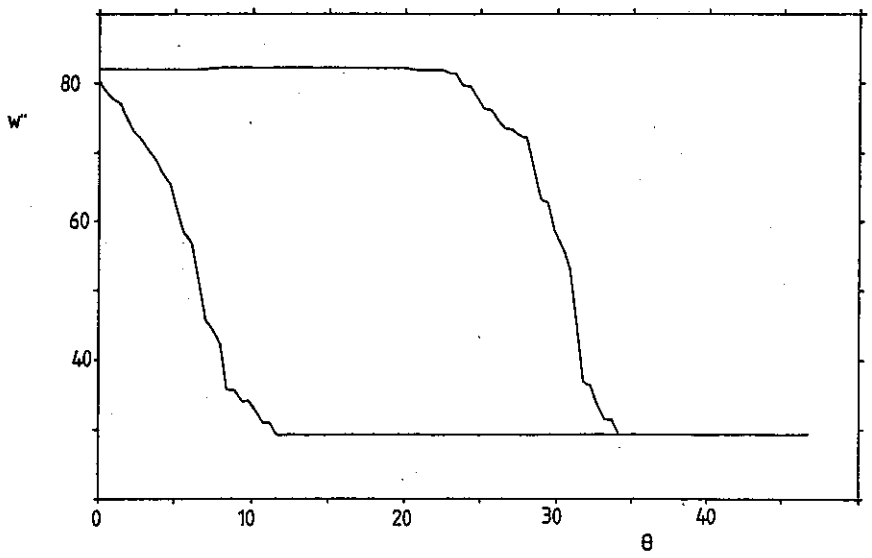

Fig. 15. The shape memory effect for bending.

plotted in fig. 14. Fig. 15 shows the shape memory effect of bar bending as a solution of incremental iterations. We do not present three dimensioinal results, as there are no comparable experimental results.

References

[1] J. Perkins (Ed.), Shape Memory Effects in Alloys (Plenum Press, New York, London, 1975).

[2] J.M. Johnson, Thermomechanical Characteristics of Nitinol, National Technical Inf. Serv. US Dept. Commerce, Springfield VA (1975).

[3] D. Goldstein, A Source Manual for Information on Nitinol and NiTi, Naval Surface Weapons Center, Dahlgren, Silver Spring (1978).

[4] I. Müller, A model for a body with shape-memory, Arch. Rat. Mec. Anal. 70 (1979) 61–77.

[5] W. Noll, On the continuity of the solid and fluid states, J. Rat. Mech. Anal. 4 (1955) 35.

[6] A. Bertram, Material systems—a framework for the description of material behavior, Arch. Rat. Mec. Anal. 80 (1982) 99–133.

[7] R. Hill, The Mathematical Theory of Plasticity (Oxford University Press, Oxford, 1950).